PNNL-28403

Pacific Northwest
NATIONAL LABORATORY

Future of Radionuclide Aerosol Monitoring Systems

January 2019

HS Miley
JL Burnett
PW Eslinger
JB Forrester
JI Friese
SJ Morris
LS Lidey
BT Schrom
JE Smart
GA Warren
AB Chepko
ME Swannick
S Stokes
CL Devoy

U.S. DEPARTMENT OF ENERGY

Prepared for the U.S. Department of Energy
under Contract DE-AC05-76RL01830

DISCLAIMER

PACIFIC NORTHWEST NATIONAL LABORATORY
operated by
BATTELLE
for the
UNITED STATES DEPARTMENT OF ENERGY
under Contract DE-AC05-76RL01830

Printed in the United States of America

Available to DOE and DOE contractors from the Office of Scientific and Technical Information,
P.O. Box 62, Oak Ridge, TN 37831-0062
www.osti.gov
ph: (865) 576-8401
fax: (865) 576-5728
email: reports@osti.gov

Available to the public from the National Technical Information Service
5301 Shawnee Rd., Alexandria, VA 22312
ph: (800) 553-NTIS (6847)
or (703) 605-6000
email: info@ntis.gov
Online ordering: http://www.ntis.gov

PNNL-28403

The Future of Radionuclide Aerosol Monitoring Systems

January 2019

HS Miley
JL Burnett
PW Eslinger
JB Forrester
JI Friese
SJ Morris
LS Lidey
BT Schrom
JE Smart
GA Warren
AB Chepko[a]
ME Swannick[a]
S Stokes[a]
CL Devoy[a]

Prepared for
the U.S. Department of Energy
under Contract DE-AC05-76RL01830

Pacific Northwest National Laboratory
Richland, Washington 99352

[a] Creare, Hanover, NH

This page intentionally left blank.

Executive Summary

In the 1990s, Pacific Northwest National Laboratory staff developed the Radionuclide Aerosol Sampler Analyzer (RASA) for worldwide aerosol monitoring. RASA won an R&D 100 award in 1998 and a Federal Laboratory Consortium tech transfer award in 2000. For the last several years, staff of PNNL and Creare have made investigations into aspects of upgrading the RASA. Key themes have been a modular approach to additional radionuclide measurements, optimizing the sampling/analyzing times to improve detection and location capability, and improving the power consumption via the use of electrostatic collection versus classic filtration. These individual efforts have been made in the context of retrofits to the existing RASA. In in this work, we consider a complete RASA redesign at a notional level. Individual studies reported here contain theory and experimental investigations, but none of these has been tested with the others, and further work is needed to verify these gains. With these caveats, this work shows that substantial optimization of detection and location capability of a network of RASA systems is possible, RASA use cases can be addressed with additional measurements, and electrostatic collection is a practical advantage, although more work is needed. The quite unexpected result of this study is that some optimization of the existing RASA is possible without any hardware changes at all.

This page intentionally left blank.

Acknowledgments

The authors wish to acknowledge the intellectual contributions of retired and deceased PNNL scientists and engineers whose enduring science legacy has made this work possible: RJ Arthur, F Brauer, RL Brodzinski, DP Brown, WH Hensley, JH Kaye, EA Lepel, RW Perkins, JH Reeves, HG Rieck, NA Wogman, and others.

The authors would also like to acknowledge international science colleagues for the encouragement and support: Matthias Auer, Patrick Grenard, Mika Nikinnen, and Dieter Wagenbach.

This page intentionally left blank.

Acronyms and Abbreviations

BEGe	Broad Energy Germanium (detector)
cfm	cubic feet per minute
CTBT	Comprehensive Nuclear-Test-Ban Treaty
ESP	electrostatic precipitator
FWHM	full width half maximum
HPGe	high-purity germanium
HVAC	heating, ventilation, and air-conditioning
IMS	International Monitoring System
MDC	minimum detectable concentration
MSDS	Material Safety Data Sheet
PNNL	Pacific Northwest National Laboratory
RASA	Radionuclide Aerosol Sampler/Analyzer
SUL	Shallow Underground Laboratory (at PNNL)
ULB	ultra-low background

This page intentionally left blank.

Contents

Figures

Tables

1.0 Monitoring History that Led to the Radionuclide Aerosol Sampler/Analyzer

Environmental monitoring of the Hanford site began in the 1940s (Singlevich 1948) including soil, water, flora, fauna, and the atmosphere. By the early 1960s, continuous monitoring of the atmosphere had begun (Perkins et al. 1990). The early approach to atmospheric monitoring employed a very high volume (500-1000 cfm or 874-1748 m^3/h) aerosol sampler collecting aerosols on a filter for up to a month, followed by a period of decay for radon daughter isotopes, then two weeks of measurement on a large, dual-crystal sodium iodide (NaI) radiation detector (Figure 1.1). This approach yielded excellent results, as seen in Figure 1.2, detecting nuclear explosions in the atmosphere of the northern hemisphere for decades. In early years shown in Figure 1.2, dual NaI was employed on 500 cfm (874 m^3/h) samples, and in later years, dual high-purity germanium (HPGe) detectors were employed on 1000 cfm (1874 m^3/h) samples. One disintegration per minute per thousand standard cubic meters (1 dpm/kSCM) is about 17 μBq/m^3. Thus, the approximately 0.05 dpm/kSCM detection limit (DL – blue line on Figure 1.2) for these systems was about 1 μBq/m^3. By comparison, IMS sensitivity range is 10-30 μBq/m^3 (red lines on Figure 1.2). The manual system of the 1980s was more sensitive than the automatic system of the 1990s, although the 1990s saw the establishment of a network of 1000-km station separation, rather than 10,000 km source-to-sampler distance employed in earlier PNNL work. This continuous monitoring activity was eventually ended post-Chernobyl due to the rarity of aboveground or leaking nuclear tests compared with the high cost of manual operation.

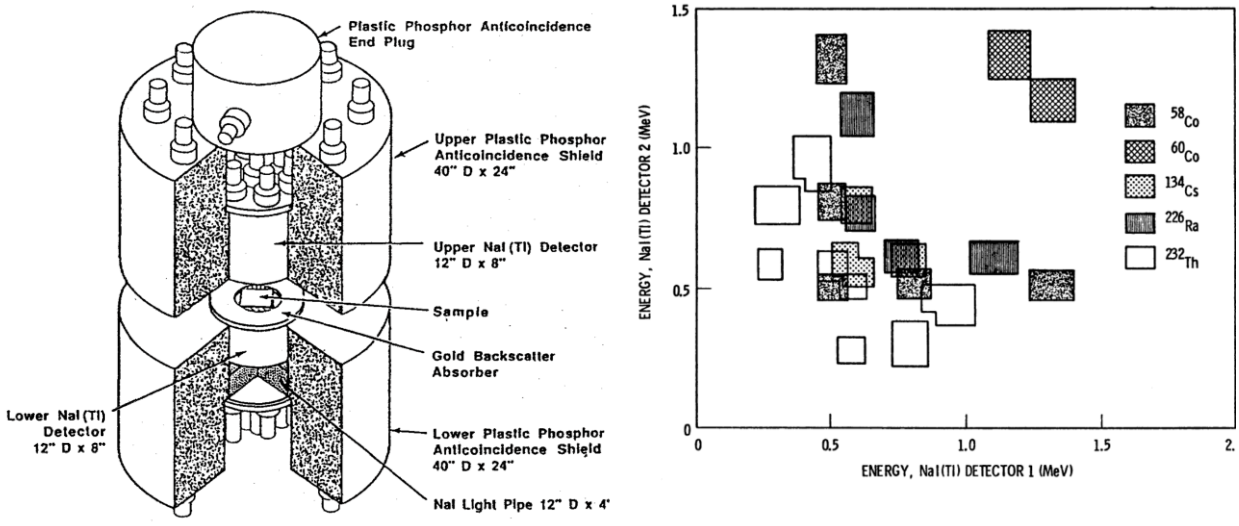

Figure 1.1. A Dual Sodium Iodide (NaI) Detector System in Use at Pacific Northwest National Laboratory before High-purity Germanium Detectors were Prevalent (Reeves 1992, Wogman 1969) and Analyzed with a Multidimensional Scheme (Brauer 1975)

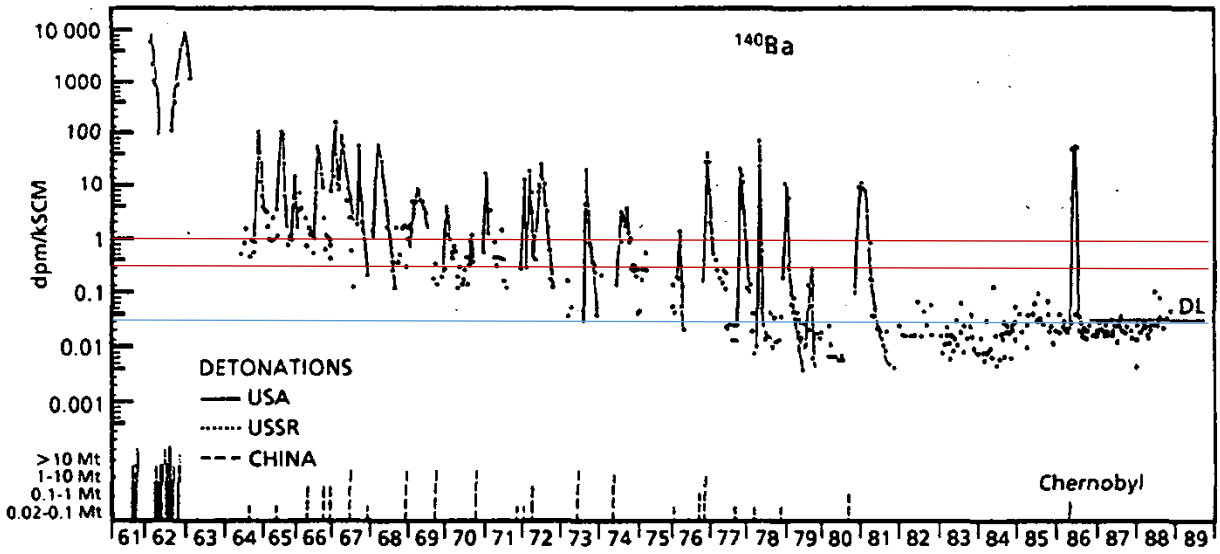

Figure 1.2. ^{140}Ba versus Time (Perkins et al. 1990) Showing Correlation with Atmospheric or Leaky Nuclear Tests.

By the 1990s, the news cycle had become a 24-hour phenomenon, and it was far from acceptable to have a month-long response time to satisfy leadership decision-making process. Also, in the 1990s it became apparent that aerosol collection and measurement functions could be automated, and by using large, modern germanium detectors, daily samples could be measured at sensitivities better than the original one-month samples on dual NaI detectors (Miley 1997). The original time period (two weeks) was selected because of the poor knowledge of the movement of the atmosphere. Event identification was based on age-dating methods using two or more isotopes and coordinating with seismic observations. In the 1990s, a faster scheme gave higher-quality nuclear results and was reasonably matched to atmospheric science calculations of transport times, with one day of collections, one day of natural radioactivity decay, and one day of measurement. Seismic location uncertainty of approximately 1000 km^2 was dwarfed by atmospheric location uncertainty of approximately 100,000 km^2. So, radionuclide measurements contributed in coordination with seismic signals to address the nuclear nature of a seismic event by the use of isotopic ratios to discriminate reactor releases from nuclear explosions.

2.0 Radionuclide Aerosol Sampler/Analyzer Use Cases

The initial purpose for the Radionuclide Aerosol Sampler/Analyzer (RASA) project was monitoring for nuclear explosions. However, the historical monitoring experience the RASA was built upon already included detection of civilian nuclear accidents. Indeed, the RASA was very useful in detecting and understanding the Fukushima nuclear disaster (Biegalski et al. 2012; Le Petit et al. 2012). While the offshore wind spared the Japan public a much larger dose, the wind blew toward the International Monitoring System (IMS) RASA in Takasaki for a short time, and the isotopes and ratios helped distant analysts understand the disaster with information of the first kind. Later, RASAs in North America reported the progress of the plume, ensuring that there was no health risk to the public, as a consequence management benefit, but also showed (Figure 3) that ratios of short-lived isotopes were useful to indicate that the event was purely a reactor release.

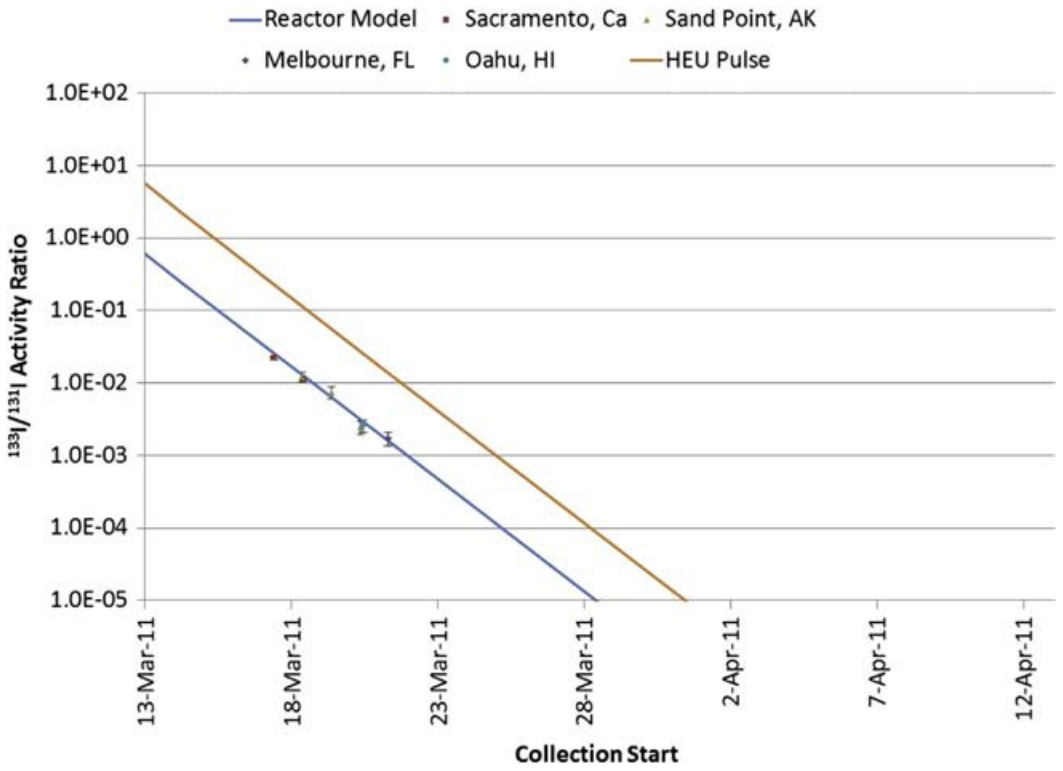

Figure 2.1. Short-lived Iodine Isotopes Measured in the International Monitoring System Show No Deviation from a Reactor Isotope Model. Shown with 1 sigma uncertainty. A small admixture (approximately 10%) of explosion iodine would cause a variation of approximately 2x in this curve.

However, these benefits came with hard lessons (e.g., in Forrester 2011) about shortcomings in the RASA design, which the authors address in Section 3.0. Further, several studies might contribute to a better design (Hubbard 2017; Morris 2017).

This page intentionally left blank.

3.0 Review of RASA Use Cases

One design lesson was about the three-day RASA timing choice. Radioactive aerosol science is relatively mature, with decades of worldwide observations. By comparison, collection and measurement of xenon isotopes is a new field. Yet, the shorter time from collection to reporting of xenon meant that 72-hour delayed aerosol data were largely ignored, even though aerosols contain valuable human health information. There are several design options that allow the RASA to cover high-level signals (atmospheric tests, reactor failure) with fast response time, and, at the same time, allow RASA to address mid-level signals (leaky underground tests, poor civilian nuclear industry operation) where natural radon decay isotopes are an impediment, and also address very low-level signals (well-contained underground tests).

These measurements can be accommodated in a single system in a modular way:

- True real-time gross radiation measurement of collected sample
  - Consequence management
  - Location refinement from time of arrival for remote explosion monitoring
- Early isotopic measurement for high-level samples
  - High-level event characterization within hours after collection, more than two days sooner
  - More sensitive for short half-lived isotopes, like ^{133}I (T1/2 = 20.8h) or ^{132}I (T1/2 = 2.3 h)
- Measurement after modest radon decay, the classic IMS use case
  - Balanced sensitivity and timeliness
- Very low background measurement after one week of decay
  - Confirmatory measurement for early-time or IMS positive detects
  - May add isotopes for low-level event characterization
  - Ten times more sensitive for longer-lived isotopes, like ^{131}I (T1/2 = 8 days).

In the 1990s, the original design of the RASA was for a moderately low-level use case (Kalinowski and Schulze 2002). In other words, the signals of interest (e.g., a leaking underground nuclear test at a great distance) were expected to be weaker than the signals created by the decay products of natural radon found in the atmosphere: ^{212}Pb, ^{212}Bi, ^{214}Pb, ^{214}Bi, and ^{208}Tl. The informal network design criteria included a 90 percent probability of detection within two weeks. The two-week time period was driven in part by slow air transport in equatorial regions. The low-level use case required three days to complete any sample. It seems likely that this use case could be updated using modern technology to achieve the same sensitivity as the original RASA from a 12-hour or perhaps 8-hour collection, thus driving a significantly smaller location uncertainty (Eslinger et al. 2016).

The Fukushima disaster provides an example of the consequence management use case. In this disaster, which released on the order of 10-kilotons-worth of fission products, signals were many times stronger than natural radioactivity, and the results were substantially later than desirable. Obviously, waiting 24 hours for negligible radon-related signals to decay was counterproductive. Consequence management could be accommodated by a radiation detector measuring radioactivity on the filter as it accumulated. This would give indication of the arrival of gross radioactivity in the air in real time. Linked to local, state, or national emergency management, the information would be invaluable in directing actions to protect life and property (Burnett et al. 2017).

Atmospheric or surface nuclear explosions are the intentional IMS aerosol use cases, and yet the Fukushima disaster showed the RASA was not optimally designed for high-level samples one would obtain from those sources. For this type of sample, the arrival time information obtained from the consequence management detector mentioned above would be valuable, but for this situation it is important to discriminate and quantify the isotopes detected to differentiate explosion signals from a reactor accident. High-activity, short-lived isotopes worked well for this with Fukushima samples, and showed that fission had stopped. One good solution to obtain this capability in a next-generation RASA could be a detector (or detector pair) measuring activity on the filter just after the end of sample collection, in what was the decay position for the original RASA. This isotopic measurement could be executed in a short period of time for a hot sample, and a variable-aperture shield for the detector could protect against very high radiation samples.

A third use case for the RASA is for slight leakage from a well-contained underground test, or a similar size leakage from civilian nuclear activity. Very low signal use cases like this would benefit from a long sample collection time and very low background detection. It has been shown that a one-week decay time for natural radioactivity before RASA measurement would allow detection limits for fission products to be improved by a factor of 10. The authors calculate that an improvement of this magnitude would have allowed the detection of ^{131}I, in the average U.S. underground leaker (Miley et al. 2009; Aalseth et al. 2009).

4.0 Notional Conceptual Design for a Next-generation RASA

The key pre-conceptual design features of the original RASA were a sample head with a collection medium that can be mechanically advanced and physically concentrated into one or more radiation measurement stations (Figure 4.1).

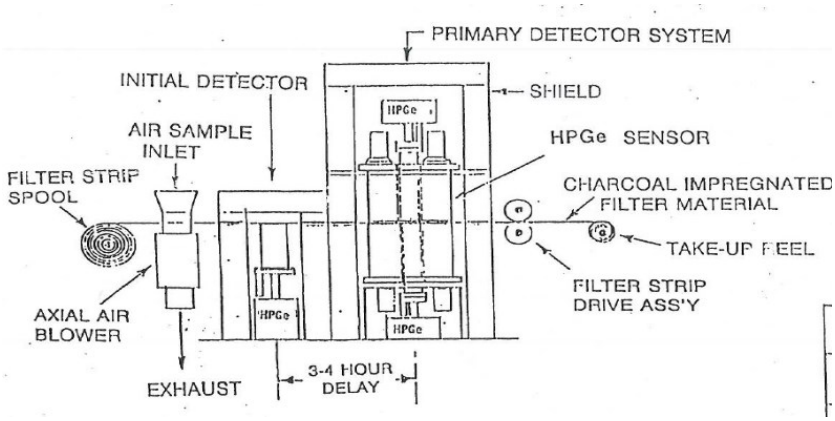

Figure 4.1. Pre-conceptual design from ST-271 proposal from PNNL to NA-22, 1992

The original RASA development (Miley et al. 1998) used a multiplexed, high-volume sample head arranged with strips of fibrous filter through which air passed, induced by a pressure drop created by a simple centrifugal blower (Figure 4.2). The filters were arranged radially in a semicircle and came together through a pair of rollers with wider, sticky strips of plastic to form a filter bundle. A pair of rollers gripped the filter bundle, and pulled it through the entire system, which advanced a section of filter from the sample head to a decay position, and then to a measurement position.

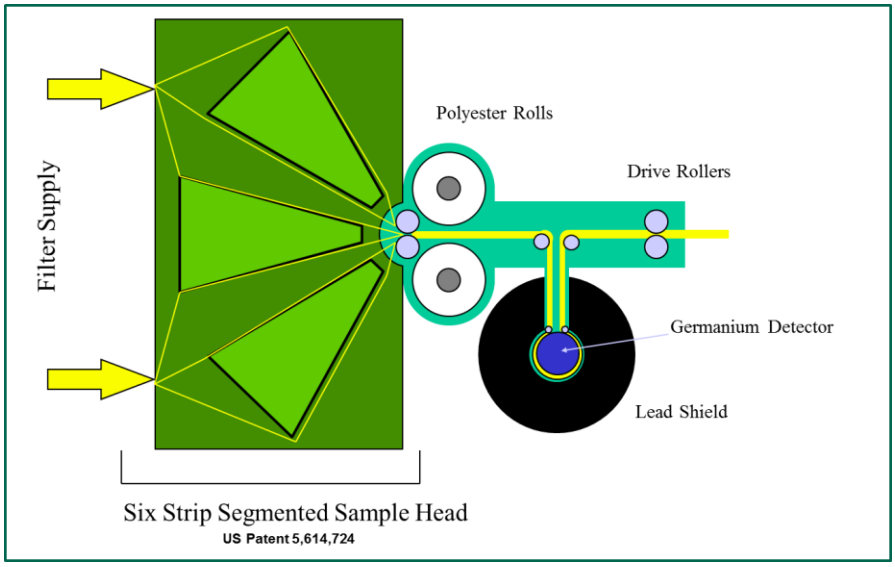

Figure 4.2. RASA Mark 4 Design Employing Six Strips of Filter, Compression Rollers with Encapsulation, a Trip Around a Radiation Detector, and an Exit, all Facilitated by a Single Pair of Drive Rollers.

In the RASA Mark 4 design, a sample head holds six strips such that a large sample area reduces the flow per square cm, reducing the pressure drop and the power needed to collect a large sample. Then, the large sample is compacted into a single strip, protected with a polyester covering, which wraps around the high-resolution germanium detector. A single pair of drive rollers powers the sample movement. The system is programmed to optionally allow a decay period between the sample under collection in the sample head and the sample under measurement in the detector. A next-generation RASA could employ electrostatic collection or a fibrous filter medium. The physical realization could accommodate all four of the measurements described in Section 3.0 such that the three RASA use cases could be simultaneously achieved or could be deployed in a modular way.

4.1 Radiation Detection

In Figure 4.3, four radiation detectors are positioned in the flow from the starting media roll to the archive media roll. Each of these represents an opportunity to tailor the radiation detection for the possible signals in various use cases (e.g., extremely elevated signals to extremely low-level signals) with various decay possibilities between each. Nominal, obvious detector choices exist, but alternatives are possible.

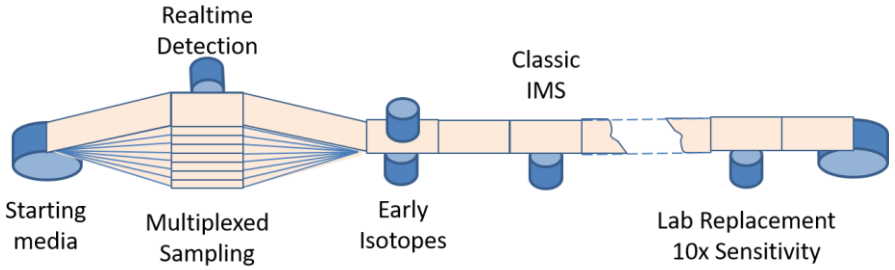

Figure 4.3. Pre-conceptual Design for the Next-generation RASA (not to scale). This concept includes all the functionality of the original RASA, but also can support signal level regimes other than a modest underground leak by the use of additional radiation detectors.

Table 4.1 presents some obvious choices and alternatives for radiation detection. In most cases, the detector with finer energy resolution is superior for differentiating and quantifying isotopes of interest from competing isotopes, like natural background radioactivity. A dual detector for isotopes that emit two or more gamma rays, can use a pair of coarser resolution detectors to achieve the same degree of differentiation, as done by Brauer et al. (1975). Dual high-resolution detectors would have been helpful to understand Fukushima samples containing more than 300 significant fission product isotopes each, or to achieve IMS-like sensitivity before allowing natural radioactivity in the RASA samples to decay.

To optimize the overall capabilities of the next-generation RASA, these and other choices should be compared to the gamut of signals possible in each scenario. Some sensors will have little utility in some scenarios. For example, the real-time detector will only see background radioactivity masking a subtle low-level signal. An ultra-low background (ULB) detector is overkill for a high-level sample. These examples lead us to favor a modular approach by location and expectations.

Table 4.1. Obvious Radiation Detection Choices and Possible Alternatives

Figure 4.3 Position	Expected Detector *Main characteristic*	Alternate Detector 1 *Main characteristic*	Alternate Detector 2 *Main characteristic*
Real-time Detection	Plastic Scintillator *Basic high count rate*	Lanthanum Halide *Some spectroscopy*	Dual NaI *High selectivity*
Early isotopes	Dual NaI *High selectivity*	Dual HPGe *Ultra selectivity in complex spectra*	
Classic IMS	Single HPGe *Balanced sensitivity/selectivity*	Dual HPGe *Ultra selectivity in complex spectra*	
Lab Replacement	ULB HPGe *Lab replacement capability*	Dual ULB HPGe *Better than lab replacement*	

Going forward, the potential selection of a solution for a radiation measurement will balance the value of data it delivers for a use case with the cost, maintainability, reliability, and complexity of analysis. The value of data is defined by the efficiency, resolution, and selectivity to detect and discriminate isotopes from each other in various scenarios.

4.2 Location Capability versus Sample Collection Time

Over the last few years, noble gas monitoring developers have sought metrics for improvement of xenon monitoring technology. One view on the focus of this work has been to exhaust every available science avenue to differentiate medical isotope production releases of xenon from nuclear explosion releases of xenon. Part of this differentiation is by location: resolving a source location to include a known medical isotope producer and/or to not include a known nuclear test site can help to focus the attention of users away from nuisance detections to where it is needed.

To this end, these developers have considered the sample collection duration as a driver of the location capability of the network. Eslinger and Schrom (2016) computed the impact on several metrics by reducing sampling intervals from 24, to 12, or six hours in simulated and real IMS results for announced nuclear tests (Table 4.2).

The values in Table 4.2 show improvements in 90 percent plausible region size, estimated event magnitude, distance to release point, and estimated release time as the sample collection time is shortened, in scenarios chosen to realistically represent remote nuclear test detection or medical isotope detection. This does not address the value of knowing the time of arrival of a plume, which can be very valuable to pro-rate the radioactivity over a partial collection time interval and to model atmospheric movement.

Table 4.2. Bayesian Estimator Performance for Different Analysis Scenarios Using Average Values of the Metrics (from Eslinger and Schrom 2016)

	Ratio of 90 % plausible region size with 6 h detections			Ratio of release magnitude (estimate/release)[a]			Distance from release point (km)			Difference in release time (h)		
	6 h	12 h	24 h	6 h	12 h	24 h	6 h	12 h	24 h	6 h	12 h	24 h
Detections	1.0	3.4	5.4	13.5	28.3	39.6	642	1341	1562	−41.0	−65.0	−65.4
Det. + mdc	0.4	1.3	3.7	3.0	5.2	4.4	244	331	324	2.8	8.2	−0.1
Set time	0.098	0.50	1.1	2.8	4.4	4.5	220	207	296	NA	NA	NA
Set Loc.	NA[b]	NA	NA	2.1	2.1	2.4	NA	NA	NA	0.5	0.4	5.1

[a] Geometric mean rather than arithmetic mean of release magnitude ratios

[b] NA denotes not applicable to the analysis scenario

4.3 Timeliness of Results

Timeliness of results is not an objective metric of performance. In the 1990s it was clear that waiting one or two months was not adequate when decisions might be needed on a days-to-weeks basis. Shorter sample collection intervals support getting early results faster. For example, an eight-hour sample collection followed by isotopic analysis immediately afterwards could result in key isotopic information in the ninth hour. The current IMS systems are nominally 72 hours from start to finish for a sample, but a "scout" spectrum transmitted after four hours of collection means that 52 hours after sample start, early results would be available.

Thinking further outside the box, the regular sample collection interval scheme could be programmed such that a rapid acceleration of the real-time count rate would trigger a system function change to, say, 10-minute collection times. Thus, hot samples would be in position to be analyzed by the early isotope spectrometer quickly, and key results could be available on the 10-minute time scale.

Other ideas would speed first analysis while preserving the system timing. For example, the real-time detector could be upgraded to provide some spectroscopy, allowing some quick characterization results

4.4 Detector-source Geometry

The term, solid angle, refers to the three-dimensional angle that an object subtends in the view of a sensor, like the human eye. At a given distance, different-sized computer monitors subtend different solid angles to the eye of the viewer, or a single monitor can subtend various solid angles at various distances. The larger the item, the easier it is to see. Inside a sphere, the sphere would subtend 100 percent of the possible solid angle, which is taken to be 4π, from the integral over ϑ and Φ. An eye inside a sphere could see nothing else, an example of 4π.

Stated simply, the authors would like to bring the radioactive source as close as possible to the sensor. Stated more specifically, the authors would like each small subdivided portion of the source to be as close to the center of mass of the sensor as possible. Ideally, the source would be inside the sensor so that no radiation could be emitted without striking the sensor. In nuclear science, the solid angle is designated $\delta\Omega$, and it varies on the range 0 - 4π. It is calculated not with integrals, but with Monte Carlo programs like MCNP or GEANT, which take into consideration the three-dimensional form of the source, detector, and the absorbing character of any materials interposed between them.

The ratio of radiation detected by a detector to the radiation which falls on the detector is called the detector efficiency, ε. So the product of the solid angle and the efficiency, εδΩ, represents a metric of the physical geometry of the source and detector.

These source-detector configurations can be selected to harmonize with an automation system for sample processing.

- The RASA Mark 4 wraparound balanced a 50-cm x 10-cm filter size as in Figure 4.4 (a) for low-power collection with a diminished δΩ for the measurement geometry and a larger high-purity germanium (HPGe) detector (ε = 90 percent relative efficiency vs the IMS requirement of 40 percent).
- The RASA Mark 2 featured a 20-cm-long by 10-cm-wide exposed filter area and a folding mechanism to achieve the 10-cm square geometry, similar to Figure 4.4 (b).
- In the case of the ST-271 proposal shown in Figure 4.1, the 10-cm square sample might conveniently match the exposed filter area to dual detectors without the added complexity of folding. But the energy needed for collection would be much higher.
- Manual systems in the IMS feature manual compression into a stubby cylindrical puck as in Figure 4.4 (c) made possible by a high-pressure press and manual sample cross-contamination protection.
- The point-source geometry of Figure 4.4 (d) is only practically achievable by soaking an absorbent resin bead with highly concentrated radioactive liquids, producing an epoxied bead of approximately 2 mm in diameter (e.g., as a calibration source). If the source is infinitesimally small, and the detector large, the detector would seem to fill about half the solid angle, or 2π.
- It is interesting to note that the HPGe detectors in Figure 4.4 (b-d) are wider and shorter than that in Figure 4.4(a) and thus achieve a higher solid angle for their respective sample shapes. This detector could be embodied by the Broad Energy Ge (BEGe) product, not available in the 1990s. A BEGe detector is less expensive while giving essentially equal sensitivity. An exception is that a BEGe is much more sensitive to lower energy gamma rays, and thus can sensitively detect more isotopes. Examples include ^{210}Pb at 46.54 keV (an isotope used in environmental research) and ^{241}Am at 59.54 keV (an isotope used for automatic gain stabilization).

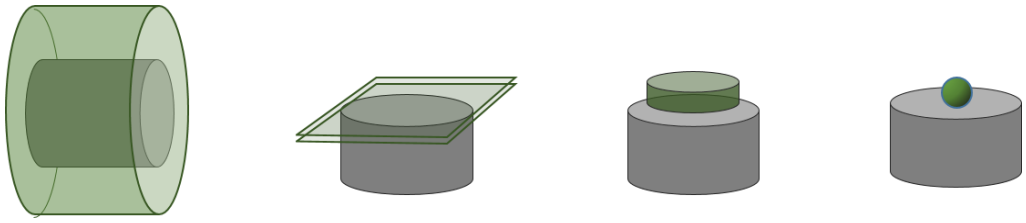

(a) **(b)** **(c)** **(d)**

Figure 4.4. Geometry Comparison of (from left to right) a RASA Wraparound Geometry, a 10-cm Square, a Compressed Puck, and a Point Source. About a factor of five separates the RASA Mark 4 solid angle from the point source, and about a factor of two separates the 10-cm square solid angle from the point source.

4.5 Power Consumption

In principle, any amount of power could be available for the proper function of the RASA. However, the lesson from Fukushima was that power was lost precisely when it was needed in a consequence

management scenario. Thus, a new design goal is to lower the system power enough to enable battery operation during a significant power failure. One possibility is to actively reduce system power use during a power failure.

The prototype RASA Mark 4 had a power design goal of 2kW for operation, but achieved roughly 1kW for a blower, 1000W for the HPGe detector cooler, and 200W for electronics. Subsequent technology improvements for the cooler (200W) and electronics (200W) would have brought the RASA Mark 4 under the design goal. Even so, 1kW is difficult to operate on practical battery systems for a substantial length of time.

At the same time, two drivers to increase the sensitivity of the RASA are to improve the sensitivity and to gather the same-sized air sample in much less time, to improve atmospheric backtracking. So, a new concept that drastically reduced the energy needed per cubic meter of air sampled would be desirable. The RASA itself was an improvement over the ST-271 concept by making the filter approximately 0.5 m^2 versus approximately 0.01 m^2.

In general, the energy needed to create V_f increases as the square of the V_f, such that

$$E_{filter} = B * V_f^2 \qquad \text{(Eq. 1)}$$

where B is a constant that incorporates the drag of the filter. Taking a second look at the energy equation above, it could be made more specific to the RASA by considering all the energy needed to be supplied for air movement. Thus, waste term is added that includes the energy wasted (heating the air or equipment) by overcoming resistance to flow through the inlet, piping, and exhaust, such that

$$E_{total} = B * V_f^2 + W \qquad \text{(Eq. 2)}$$

W is not a trivial amount of energy in some RASA installations, and the original RASA developers specified large diameter ducting and large inlets to reduce W. In most air samplers, $B * V_f^2$ is much larger than W. However, as a goal $B * V_f^2$ should be made similar or smaller than W, such that the filtration segment of the ducting requires no more power than others (Figure 4.5).

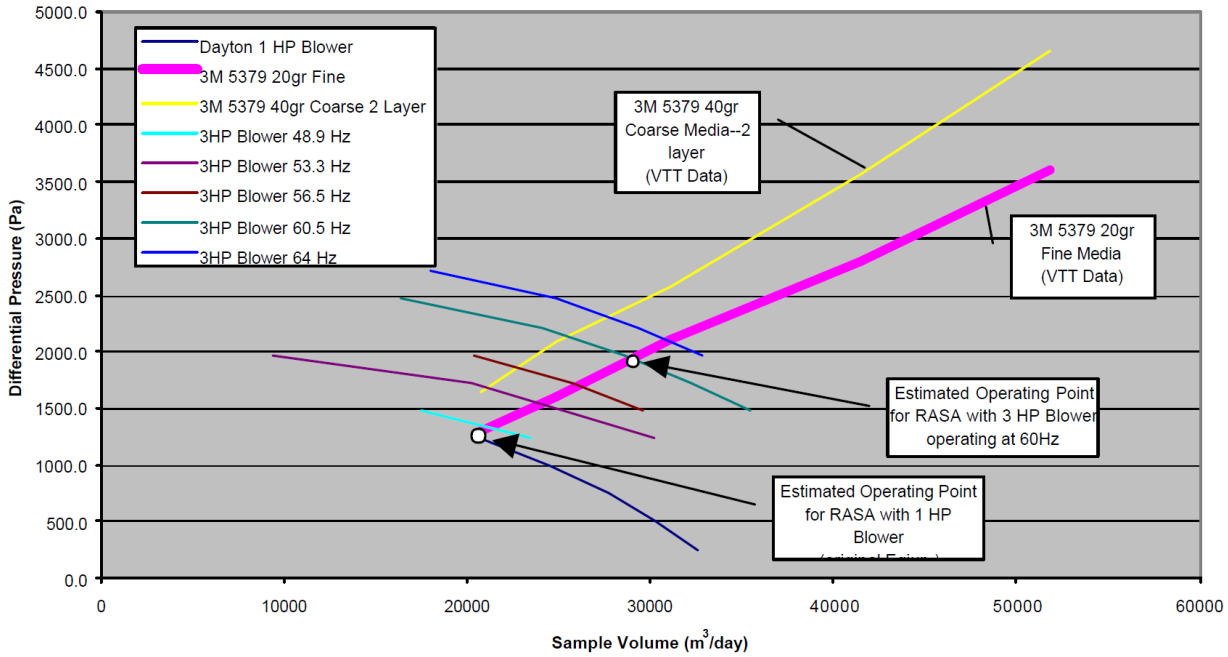

Figure 4.5. Certain RASA Filters Used with Possible RASA Blowers (from Thompson et al. 2002)

This could roughly be paralleled with $dP_{total} = dP_{RASA} + dP_{filter}$, where 1300 Pa = 240 Pa + x, so thus the pressure drop of the filter alone is around 1000 Pa or approximately 4 inches of H_2O. The 240 Pa developed by a RASA with no filter can be thought of as representing the resistance to air flow (at approximately 1000 m^3/h) presented by the ducting and torturous path through the RASA sample head. In reality, with no filter, the air flow is probably quite a bit higher, and the dP for the no-filter RASA goes up higher than the contribution would be for the rest of the RASA with the filter in place. Thus 240 Pa is an overestimate for the no-filter RASA.

A completely different way to collect particulate would be electrostatic precipitation. The action of an electrostatic precipitator (ESP) is very simple compared to the flow of air through a filter. Electrons are discharged into air being drawn into the precipitator from a corona wire. Either by direct bombardment or by diffusion, the electrons come into contact with the particles in the air and charge them. Several charges can be attached to a single particle, and a high percentage of the particles need to be charged (saturation). The particles are then swept between many parallel plates alternately at ground potential and at a positive voltage. The excess electronic charge draws the particles to the positive plates where they are trapped.

4.6 Theory of Operation of an Electrostatic Precipitator versus Commercial Off-the-shelf Testing

At the simplest level, air passes charged wires, which attach electrons on passing particles, then the air with these charged particles passes between parallel plates alternating ground and positive charge. The particles have a negative charge, and a large positive potential is applied to the plates, which sticks the particles to the plates.

The probability of collecting a particle is then proportional to the percentage of particles ionized (Pi – related to the negative corona discharge voltage), the electrostatic force applied (Fe – related to the number of electrons we stick on each particle and the positive voltage on the plates), and the length of

time the particles are between the plates (Tp – for any velocity of air, the plates need to be wide enough to allow particles to drift all the way to the plate).

$$P \alpha Pi * Fe * Tp \qquad \text{(Eq. 3)}$$

Overall, the resistance to airflow of the system shown in Figure 4.6 is quite low, similar to a piece of ducting of similar dimensions. Low pressure differential in the system also opens up new possibilities in high volume with simple, cheap, low-power blowers as used in heating, ventilation, and air-conditioning (HVAC) systems. The RASA collects particles from about 1000 m^3 per hour, which is about 600 cubic feet per minute (cfm) in the units of HVAC. A simple 12-in. HVAC blower can move about 3000 cfm with a pressure differential, again in HVAC units of 1 inch of water (1 in. H_2O).

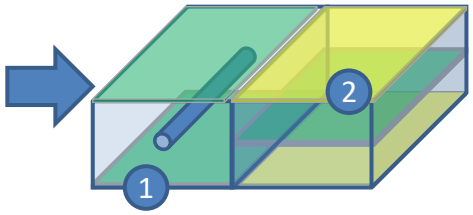

Figure 4.6. A Simplified Notional Design of a Precipitator Showing (1) a Corona Discharge Wire at -V1 between Grounding Plates and (2) Two Plates at +V2 on either Side of a Ground Plate. In practice, limitations on arcing limit V1 and V2 and the design of the system.

A quick survey of available commercial electrostatic filtration systems show that duct-friendly designs that claim efficiencies close to Comprehensive Nuclear-Test-Ban Treaty (CTBT) requirements (80 percent efficiency for 0.2 micron particles) with flow rates as high as 2000 cfm, exist. Consider for example, the Honeywell F300E1035 as shown in Figure 4.7. It claims a 2000 cfm flow rate max, fits a large duct of about 60 cm x 50 cm, and for about 500 feet per minute face velocity (2.6 m/s) claims an efficiency nearly good enough to meet IMS minimum standards. This is about twice the flow rate of the RASA, and yet should only add 0.05 inches of water pressure drop to the RASA ducting, as seen in curve 3 of Figure 4.9. Because of the relationship of time inside the parallel plates to the efficiency, a lower efficiency at higher face velocities is expected.

Figure 4.7. Honeywell Electrostatic Air Cleaner F300E1035

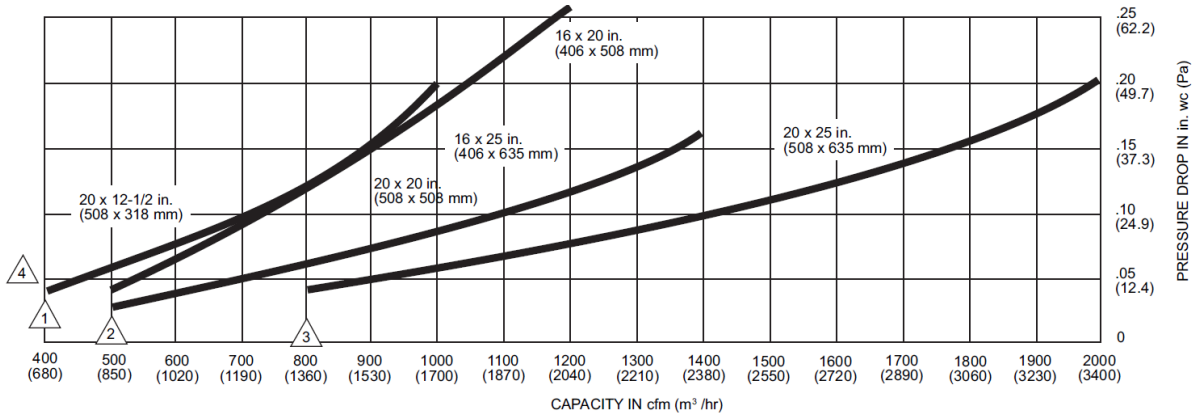

Figure 4.8. Volume Capacity versus Pressure Differential in Honeywell Electrostatic System. The CTBT minimum requirement of 500 m^3/h would be 294 cubic feet per minute, and is off-scale to the left. Thus the pressure drop at even twice the CTBT flow rate would be about 0.05 inches of water or about 12 Pa.

Figure 4.8 shows that commercial systems like the Honeywell have a negligible air pressure drop, perhaps as little as 1 percent of the value of the RASA filter. The possibility of flow loss due to clogging is even less, but saturation of the collection surface should be considered.

Thus, filling in the pressure drop equation $dP_{total} = dP_{RASA} + dP_{filter}$ with estimates, the new pressure drop would be dP_{total} = 240 Pa + 12 Pa. About 80 percent of the dP and thus about 80 percent of the power requirement for the air movement would be gone. Also, using the no-filter RASA estimate for the waste power implies that the drag in the sample head does not change, so it is possible that a larger proportion than 80 percent of the power would be eliminated.

In traditional ESP, the particulate collects on metal plates. In principle these plates are periodically wiped; ultrasonicated; acid-etched; or, in a large factory air-cleaning applications, automatically rapped by a hammer to remove gross quantities of particulate. A RASA ESP implementation would need a different method of collecting the particulate. A system that includes a method to move the particulate past a radiation detector and into a form that can later be processed chemically is necessary. The most promising method is to pass a conductive film over the metal plates or perhaps using conductive films or foils as the collection plate that moves through the collection area.

4.7 Using a Laboratory to Back up a Station Measurement

When a RASA makes a measurement that shows an anomaly, say, because of the presence if fission products or the absence of natural radioactivity, there is no possibility of a repeat measurement at the station – the RASA can only move forward to new samples. The anomalous sample must be manually retrieved and sent to a laboratory for a secondary measurement. This re-measurement serves to confirm the original, but, if done with extra sensitivity, may add additional isotopes that through isotopic ratio study could:

- Fix the time when fission took place,
- Estimate the time the sample entered the atmosphere, or
- Screen out uninteresting sources, such as leakage from civilian power generation.

The first two pieces of information are very powerful in improving the atmospheric backtracking ability, and laboratory capability is therefore important.

Today, the IMS network of RASA stations is backed up by a 16-laboratory network. A small percentage of samples are sent to laboratories for quality assurance and quality control of the stations. A few times a year samples exceed thresholds of interest, and must be split and sent to two laboratories. This process is enabled by expensive and controversial schemes that include laboratory selection, sample splitting, border-crossing delays, shipping time, inaccessibility of remote stations, laboratory operation hygiene, laboratory proficiency tests, and the ultimate archival of these. Each of these problems could be resolved by placing a second, low-background detector at the station to automatically re-measure every sample.

A secondary detector that could replace the laboratory measurement might cost about $500,000 per station in capital costs, but would rapidly pay for itself in reduced overall costs. The IMS laboratories have no utility for remote and polar stations, which are so remote that samples cannot be sent for re-measurement. At least on a modular basis for remote stations, the laboratory-replacement detector seems like a mandatory design component of a next-generation RASA.

5.0 Electrostatic Precipitation Considerations

Electrostatic precipitation offers an approach to aerosol collection that can provide greater operational flexibility to accommodate future radionuclide aerosol monitoring requirements. The performance can be dynamically adjusted by controlling independent parameters, such as flow rate and the electric field strength within the precipitator. This control allows operators to enhance or reduce particle collection in real time, adjusting to changing radionuclide load conditions, and operating in a low-power mode during times of limited power availability.

An ESP can accommodate significantly increased flow volumes, which can increase the instrument sensitivity and provide design flexibility. The open flow channels in an ESP result in very low pressure drops and require much less blower power than conventional filters. While ESPs require high voltages to operate, the current is very low, so that the supplied electrical power is typically low. This approach to radionuclide collection will significantly reduce system power, increase sample collection, and improve instrument detection sensitivity.

5.1 Electrostatic Precipitation Design

A new radionuclide collection system is under development by Creare, LLC, based on a standard wire-plate ESP implementation (Figure 5.1). Flow is drawn into a duct consisting of a set of parallel channels. The new system lines the channel walls with sheets of thin, metallized plastic. The thin, metallic layer on the film provides the electrical properties to serve as a collector electrode, and the flexibility of the plastic sheets allow them to be scrolled through the precipitator volume, sealed together at the edges, folded into a small package size, and presented to a detector or spooled for later analysis. This approach minimizes the cross contamination of successive samples and minimizes the surfaces within the precipitator volume that are continually exposed to the aerosol flow. The ESP system sizing can be adjusted to accommodate different installation requirements: a minimum flow length is necessary to achieve efficient particle collection, but this can be traded somewhat with power consumption by employing a higher electric field to accelerate particle collection. Additional flow channels can be installed to accommodate even higher flow volumes, but this also must be traded against the sample sheet folding complexity and final sample size constraints.

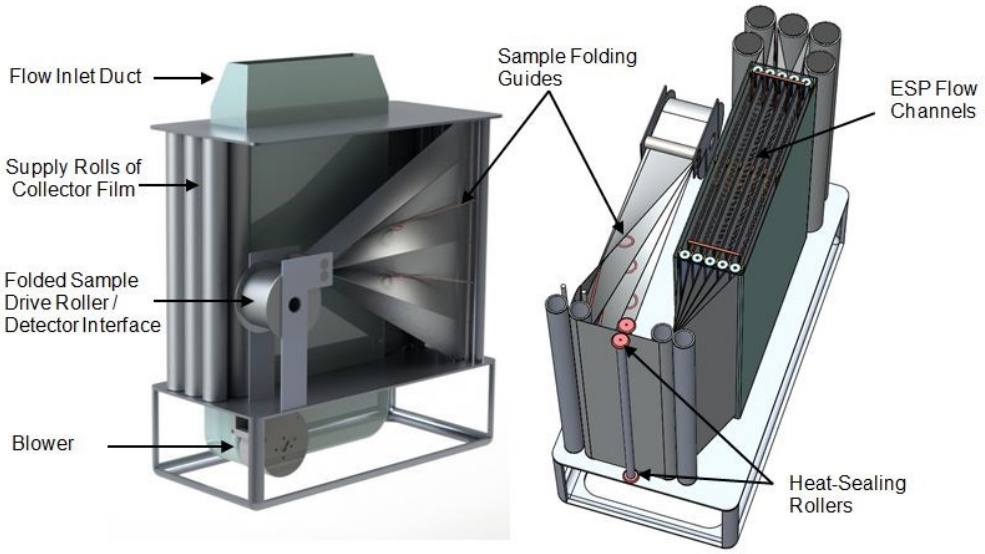

Figure 5.1. Concept Design of Electrostatic Precipitator for Radionuclide Collection

A set of thin-wire discharge electrodes is arranged along the center of each flow channel. A high voltage, on the order of 8-15 kV, is applied to the discharge electrodes, creating a strong electric field between the wires and the collection sheets. As gas flows through the system, a corona of ionized gas molecules develops around each discharge electrode, electrostatically charging the aerosol particles entrained in the flow (Figure 5.2). Once charged, the particles are drawn by the electric field toward the collection sheets, where they remain through a combination of electrostatic and van der Waals forces. The electrical force is countered by drag and dispersive turbulent forces on the particle, so an ESP must be designed with a long enough flow residence time for the particle to build charge and migrate to the collector. Particle resistivity also plays a role in ESP performance—too high of resistivity can reduce electric field strength and lead to a back-corona discharge if the dust layer builds up too much, whereas a low resistivity results in easier re-entrainment of particles back into the flow. Typical atmospheric aerosol resistivity falls into the moderate-to-high range, although this varies with composition, temperature, and relative humidity.

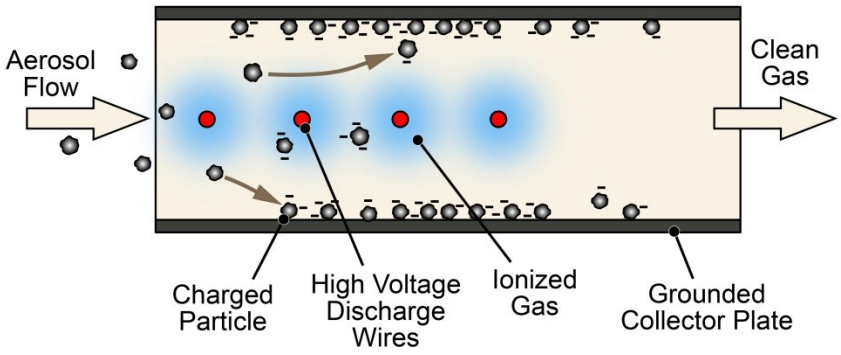

Figure 5.2. Fundamental Electrostatic Precipitation Operation

5.2 Trade-Space of ESP-Based Radionuclide Collection System

Creare has developed a system model to predict ESP performance for radionuclide collection using literature-based models for particle charging ESP current, and particle collection efficiency (Cochet 1961; Cooperman 1960; Cooperman 1981; Parker 1997). The model in conjunction with subscale testing is guiding the design of a full-scale prototype collector that will be tested in 2019. The key design trades for an ESP-based radionuclide collection system balance particle collection efficiency, total sample flow volume, system power consumption, system size, and sample handling complexity.

5.2.1 Sample Collection versus Sample Flow Rates

The CTBT radionuclide particulate monitoring station minimum requirements specify a filter particle collection efficiency of 80 percent for particles of diameter 0.2 µm at a minimum sample flow rate of 500 m^3/h for a 24-hour sampling period. This baseline can be equated to a minimum total sample air volume of 12,000 standard cubic meters. By placing a requirement on the filter flow-through particle collection efficiency rather than on the total sample volume particle collection, the potential for significant gains in instrument sensitivity may be lost. For example, because an ESP has a much lower pressure drop compared to a traditional filter, the system can operate at much higher sampling flow rates for a given input power than current systems such as the RASA. With all other operating parameters held constant (such as ESP operating voltage), as the flow rate through the system increases, the flow-through particle collection efficiency decreases. However, even at a lower flow-through efficiency, because the total sample volume can be much larger, the overall number of collected particles in a sample can be two to four times greater than the CTBT requirement (Figure 5.3). This can lead to substantial improvements in instrument sensitivity. For example, an ESP system operating at 90 percent particle collection efficiency at a sampling rate of 1000 m^3/h will acquire an actual sample quantity that is a little over twice the CTBT requirement. The same ESP system might only achieve 60 to 70 percent particle collection once the sample rate is ramped up to 2000 m^3/h, but this will yield an actual sample count that is 3.5 times greater than the requirement.

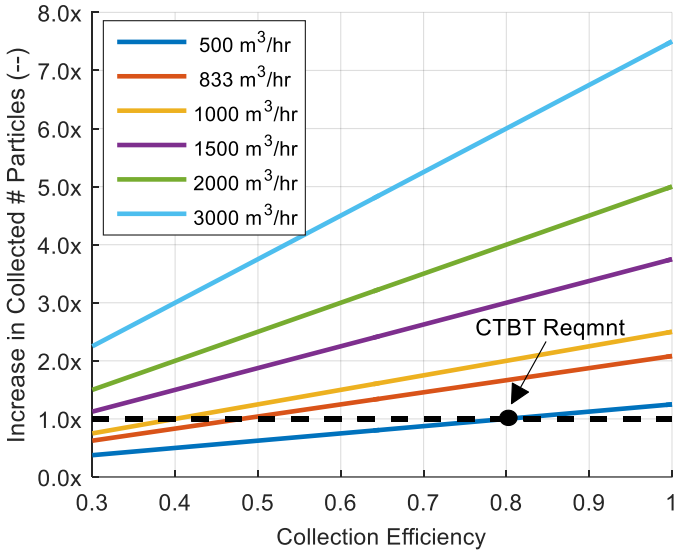

Figure 5.3. Relative Increase in Total Number of Collected Particles over a Baseline 12,000 m^3/day Sample Volume (500 m^3/h at 80% Filter Particle Collection Efficiency) for Different Flow Rates and Filter Collection Efficiency Requirements

5.2.2 ESP System Performance versus Sizing

An ESP's particle collection performance is based on the amount of charge transferred to a particle, a particle's residence time within the unit, and the strength of the electric field that draws the charged particles to the collector surfaces. The residence time is a function of the sampling air flow rate, the number of parallel ducts within the ESP, and the duct sizing. A shorter ESP flow length can be balanced by increasing the electric field strength (and thus power consumption) up to functional limits that prevent direct arcing. An ESP-based radionuclide collection system design can be adjusted to accommodate different installation and operational requirements. Figure 5.4 shows how ESP collection performance varies with flow duct length for a particular ESP design configuration that includes several parallel flow ducts. Note that collection efficiency is shown for a particle size of 0.25 μm, which is the most challenging particle size for an ESP because of charging regime crossover points dependent on particle size—η of <0.25 μm and η of > 0.25 μm particles are higher. While ESP power consumption is difficult to model accurately, rough estimates for this design (overall ESP volume approximately 0.5 m x 0.5 m x 1.0 m) range from 800 W at 1000 m^3/h to 1.1 kW at 2000 m^3/h, including blower power. Therefore, this system can achieve a 3.5x increase in total sample collection over CTBT requirements (operating at η = 70 percent at 2000 m^3/h) for roughly half of the 2.2 kW power consumption of the RASA system.

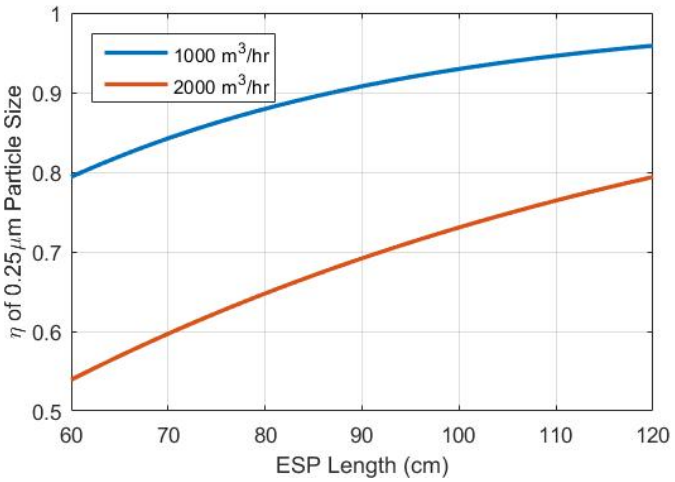

Figure 5.4. Flow-through Particle Collection Efficiency versus ESP Duct Flow Length for Varying Flow Sample Rates (for a Given ESP Design and Electric Field)

5.2.3 ESP Radionuclide Collection System Operational Flexibility

Employing an electrostatic precipitator for radionuclide collection will offer greater flexibility for operators to respond to evolving events such as the Fukushima incident. In a conventional filter, sample acquisition quantities can only be adjusted by varying the air flow rate through the filter and the total acquisition time. Flow rates can only be increased as much as power source limitations and the pressure drop through the filter allow. Alternatively, in an ESP, both the flow rate and the electric field strength (or applied voltage) can be dynamically adjusted, allowing a greater operating range for sample acquisition. In a power-limited situation, the ESP voltage can be dialed back to drastically reduce power consumption while still maintaining some level of sample acquisition. Alternatively, with high power availability, both flow rate and voltage can be increased to achieve much higher sample quantities. Figure 5.5 presents the potential range of performance and estimated power requirements for varying flows and voltage levels in one potential ESP design.

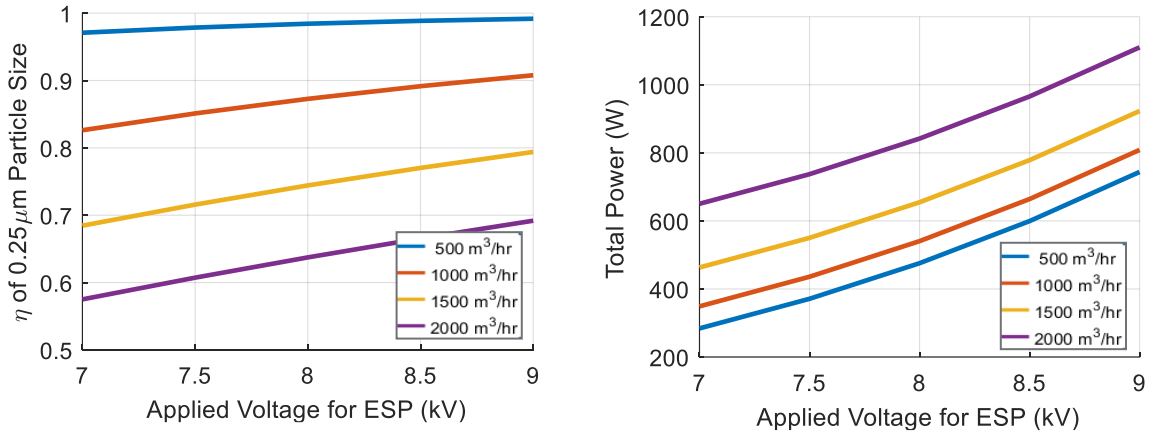

Figure 5.5. Collection Efficiency versus ESP Voltage (left) and Total Power versus ESP Voltage (right) for Varying Flow Rates in an ESP Design Concept for Radionuclide Collection

5.2.4 ESP Radionuclide Collection System Sampling Handling

The ESP radionuclide collection system currently under development employs flexible, conductive sheet material as the particulate collection surfaces. After sample acquisition has completed, these sheets are automatically withdrawn from the precipitator volume, sealed together at the edges to prevent particle loss or contamination, and then folded for presentation to the radionuclide detector. The collector sheets are much thinner than the filter paper materials used in the RASA system, leading to the potential for smaller sample packets and improved detector interfacing. The existing RASA collection system currently presents the sample to the detector in a 10-cm-wide, approximately 40-cm-long strip of filter material that is wrapped around the detector circumference. Presentation of a narrower strip (i.e., < 10-cm wide) or a small packet that is instead placed on top of the detector can significantly increase overall instrument detection sensitivity.

The form factor of an ESP drives system sizing towards larger collector sheet areas to improve collection efficiency and reduce power. However, increasing the ESP size or number of flow ducts increases the complexity of the sample folding operation and at some point limits the final achievable sample packet size due to the number of required folds in the material. Because the system must function autonomously, the overall ESP-based radionuclide collection system must balance collection performance with sample-handling complexity. Table 5.1 presents a range of sample handling approaches that illustrate the potential gains, trade-offs, and challenges. A smaller ESP with a lower flow-through particle collection efficiency and smaller collector sheets may provide the best overall net increase in instrument detection capability by producing a much smaller sample packet. The actual sample packet dimensions will depend on the final duct dimensions and exact folding mechanism employed to achieve sample size reduction.

Table 5.1. Sampling Handling System Trade-offs

Sample Format	Folding System Size / Complexity	Detector Efficiency Gain (εδO)
~10 cm Wide Strip; Wrap Around Detector	Least Complex, Allows for Larger Sheets (up to at least 1 m) or More ESP Ducts	Same as RASA (1X)
~5 cm Wide Strip; Wrap Around Detector	More Complex, Limits Sheet Size to < ~1 m	Perhaps 30% more efficient than RASA. Computations needed.
<10 cm x <10 cm Packet; On Top of Detector	Most Complex, Limits Sheet Size to < ~1 m (Dependent on System Specifics)	About 2x more efficient than RASA

5.3 Radiochemistry of Aluminized Mylar

There is a CTBT IMS requirement that filter media used in the IMS be dissolvable. This is because, in classic monitoring, samples were chemically separated to overcome the inability of first generation radiation detectors to discern one isotope from another using gamma energy analysis. This lack of selectivity has been addressed by detector physicists by the use of coincidence detection and since the 1970s by the use of high-energy resolution detectors such as HPGe. Nevertheless, chemical separation still provides enhanced analysis even for HPGe use and is still a desirable characteristic of future RASA samples.

Chemists investigated this potential RASA collection material from the classic dissolution perspective, as discussed in Appendix A. It represents some challenges that would have to be considered further, but there is good reason to believe it would be successful. However a significant possibility exists for chemically or physically removing the collected particulate material without completely digesting the conductive surface and plastic substrate. This would avoid completely the issue of radioactive materials in the aluminum, discussed below.

Chemical digestion experiments were done using wet ash and dry ash approaches. At this time it is difficult to render a full assessment of the suitability of aluminized Mylar® (registered trademark of DuPont Teijin) as a filter collection material from a chemical processing perspective. A few common techniques were not applied to these samples due to safety concerns and/or time constraints: perchloric acid ($HClO_4$; safety concern), aqua regia (3:1 concentrated HCl:concentrated HNO_3 mixture), hydrofluoric acid (HF), and multi-acid mixtures such as $HF/HClO_4/HNO_3$. Based on the tests completed and from our historical process knowledge, the aluminized Mylar would bring new complications during processing. The filter media currently used in RASA units is known to dry ash down to an easily digestible solid after a long, slow dry ashing procedure. The aluminized Mylar clearly did not dry ash down to a similarly easily digestible solid (see Appendix A).

Additional consideration for working with aluminized Mylar would be the handling of the material to get it from sampling to processing. Mylar materials become charged, which could make handling a loaded sample hazardous from a contamination standpoint. The size of the final material would also need to be evaluated for appropriately sized beakers or furnaces. More experiments and the appropriate Material Safety Data Sheet for this material would be necessary to fully assess this paper for suitability as a filter material for chemical processing.

The radionuclide content of an aluminized Mylar sample was analyzed using a low-level gamma-spectrometer within the Shallow Underground Laboratory (SUL) at Pacific Northwest National Laboratory (PNNL) (Aalseth et al. 2012). The SUL is optimized for low background measurements, with a calculated 30 m of water equivalent (mwe), which results in approximately 100 times fewer fast neutrons and six times fewer muons. In this instance, a Canberra Broad Energy Germanium (BEGe) detector was used in a configuration quite similar to Figure 4.4(c). The BEGe detector combines the spectral advantages of low energy and coaxial detectors, with an energy range from 3 keV to 3 MeV and optimized energy resolution and efficiency. The system is equipped with a cosmic veto system (Burnett and Davies 2014) to further improve sensitivity by reducing the detector background by 25 percent.

A 42.9 g sample of the aluminized Mylar was compressed into a cylinder (55 mm diameter x 22 mm height) and measured for eight days The resulting gamma spectra analysis indicated trace levels of naturally occurring radionuclides from the ^{238}U and ^{232}Th series (Table 5.2). The activity of these radionuclides ranged from 3.7 x 10^{-4} Bq g^{-1} to 1.2 x 10^{-2} Bq g^{-1}.

A comparison was made with a 40.0 g sample of compressed RASA material, which was measured using a certified IMS gamma-spectrometer (Greenwood et al. 2017) in the SUL for 7 days. This sample showed only measurable ^{40}K at 2.6 x 10^{-4} Bq g^{-1}. All other radionuclides were at the minimum detectable concentration (MDC) level, typically an order of magnitude lower than for the aluminized Mylar sample. This would indicate the aluminized Mylar contains an increased amount of intrinsic radioactivity than the current RASA material.

The authors suspect that this increased level would not affect daily IMS samples, but would indeed affect laboratory re-measurements or a second, low-background measurement by a future RASA. More investigation is needed to determine if this is a substantial effect or if it could be remedied by selecting an alternative aluminum source.

Table 5.2. Measured Radionuclides within Aluminized Mylar Sample

Nuclide	Energy (keV)	Aluminized Mylar			Standard RASA Filter		
		Activity (Bq/g)	Uncertainty (%)	MDC (Bq/g)	Activity (Bq/g)	Uncertainty (%)	MDC (Bq/g)
^{40}K	1460.8			3.5E-03	2.6E-04	53.1	4.5E-04
^{234m}Pa	1001.0	1.2E-02	12.1	6.7E-03			2.5E-03
^{226}Ra	186.2			6.2E-03			6.2E-04
^{214}Pb	351.9	1.4E-03	3.2	1.6E-04			1.6E-04
^{214}Bi	1120.3	2.2E-03	7.1	6.0E-04			2.0E-04
^{210}Pb	46.5			2.9E-03			4.1E-03
^{228}Th	84.4	6.0E-03	9.7	3.0E-03			1.7E-03
^{228}Ac	911.2			2.9E-04			8.8E-05
^{224}Ra	241.0	6.4E-03	7.4	2.3E-03			1.1E-03
^{212}Pb	238.6			5.5E-04			5.6E-05
^{212}Bi	727.3			1.0E-03			3.0E-04
^{208}Tl	2614.5	3.7E-04	10.9	1.2E-04			2.6E-05
^{235}U	185.7			3.9E-04			3.9E-05

MDC = minimum detectable concentration, RASA = Radionuclide Aerosol Sampler/Analyzer

5.3.1 Minimum Detectable Concentration versus Design

The topics of radiation detection resolution, sample collection time, source-detector geometry, and sample volume versus power have been covered in other sections. In this section, the authors develop the design metric that connects all of these and that most closely relates to the needs of the user, MDC. The impact of varying some of these parameters will also be examined, taking far greater liberty than in the 1990s in the RASA design.

The minimum detectable activity is a measure of the sensitivity of a particular detector system. For the RASA, the minimum detectable activity can be defined as the lowest amount of activity that could be detected given the detector operation and fluctuations in background counts. A general explanation for determining detection limits can be found in Currie (1968) for a variety of different scenarios. The approach for determining the sensitivity of the RASA is based on the approach of Currie (1968), with an assumption of 5 percent false positives and 5 percent false negatives.

5.3.1.1 The MDC Equation

The measurements are reported as a concentration with units of $\mu Bq/m^3$ and so the MDC is based on the minimum detectable activity. The MDC equation is then:

$$MDC = \frac{1}{\lambda \times Br}\sqrt{\frac{2 \times BckCnt \times FWHM}{\epsilon \times d\Omega \times V \times t}} \qquad \text{(Eq. 4)}$$

In Eq. 1 MDC, λ is the decay constant of the isotope being measured and Br is the branching ratio of the energy level of interest for the decay. These two terms depend on the isotope, but not on the design of the detector. The full width half maximum (FWHM) generally denotes the full width of the peak at half of its maximum height, but in this context, it denotes the sum of the counts in the portion of the energy spectrum containing the peak associated with the isotope. The term BckCnt denotes the background counts in the region of the peak (counts not caused by the presence of the isotope of interest). The detector efficiency is a function of the type of material chosen, ϵ, and the counting geometry efficiency, dΩ. The sample air volume is denoted by V, and the sample count time is denoted by t.

Lower values of MDC indicate better detector performance. Thus, when designing a new system using the same type of detector material (such as high-purity germanium) as a previous system, the designer can lower the MDC by selecting a favorable combination of BckCnt, dΩ, V, and t.

Systems used in the IMS must be able to report a sample concentration within 72 hours of the start of sample collection. The current RASA uses a sample collection time of 24 hours, a decay time of 24 hours, and a counting time of 24 hours. The decay time is important, because it improves the MDC by allowing a large portion of the background-inducing radon decay products to decay before the sample is measured (Miley 2009). The most significant contributor to the background counts is ^{212}Pb (LeppÄnen and Toivonen 1996), which has a 10.64-hour half-life. Using a 72-hour reporting time requirement, if the sampling time and counting times were both reduced to 12 hours, then the decay time could increase by 24 hours, and the background counts would decrease to 21 percent of the previous background counts. If the flow rate were unchanged, then the sample volume would be reduced by a factor of two. If the current RASA were operated on a 12-hour collection and counting time basis, the MDC would reduce to 0.92 of the current value. If sample collection times were shortened to 8 hours, the MDC would rise by a factor of 1.06. Although shorter collection times may lead to higher to a MDC, the shorter collection time is associated with better location precision when using the sample concentrations in a source-term analysis

(Eslinger and Schrom 2016). Thus, for the IMS, there is a desire to reduce the sample collection time as much as possible.

5.3.1.2 Varying Some Design Parameters

The current RASA configuration wraps the filter paper around a cylindrical detector. This configuration has a dΩ of about 0.2 relative to the optimal configuration of a highly compacted filter paper sitting on one end of a cylindrical detector. If the filter paper were folded just enough to sit on the end of the cylindrical detector, then dΩ would increase to 0.5.

Based on 8,984 IMS samples taken over the last six years, the average volume of air collected by a RASA is 21,623 m^3 for 24-hour collection periods. This corresponds to an average flow rate of about 900 m^3/h.

The change in the MDC (expressed as a multiplier on the MDC for the current RASA) for different design configurations is shown in Table 5.3. The sample volume is provided as a multiplier to the current air flow rate of 900 m^3/h. The background counts for different decay times are adjusted using the decay constant for ^{212}Pb. Row A of Table 5.3 shows the current configuration, thus has a MDC multiplier of 1. This analysis suggests that the current RASA would have slightly improved performance (multiplier of 0.92) if it were operated with 12-hour collection and counting times.

Table 5.3. Impact of Different Design Configurations on the MDC of the Classic IMS Measurement Position

	Geometry	Flow Rate	Sample & Count	Decay Time	MDC Factor
A	0.2	1	24	24	1.00
B	0.2	2	24	24	0.71
C	0.2	3	24	24	0.58
D	0.2	1	12	48	0.92
E	0.2	2	12	48	0.65
F	0.2	3	12	48	0.53
G	0.2	1	8	56	1.06
H	0.2	2	8	56	0.75
I	0.2	3	8	56	0.61
J	0.5	1	24	24	0.63
K	0.5	2	24	24	0.45
L	0.5	3	24	24	0.37
M	0.5	1	12	48	0.58
N	0.5	2	12	48	0.41
O	0.5	3	12	48	0.33
P	0.5	1	8	56	0.67
Q	0.5	2	8	56	0.47
R	0.5	3	8	56	0.39

5.3.1.3 Highlights of Variations

In Table 5.3, Row A represents the current RASA design which operates on a 24-24-24 time basis. Row R represents an improved geometry, flow rate, and maximized decay time, still within the 72-hour IMS requirement. The MDC factor of 0.39 indicates that the MDC would be only 39 percent of its previous value, more than a factor of two more sensitivity, but adding the benefits of shorter integration time and better source location. If this was achieved with ESP, it might be at substantially lower total power, as well, and achievable on battery power.

A few other rows merit comment:

- Row G suggests that today's RASA would only have 6 percent worse MDC if operated on an 8-56-8 time basis. With a general improvement in air volume or a cosmic ray veto system to recover the nominal required MDC, today's RASA could be better at locating sources.
- Row L implies that a folded geometry versus wraparound and tripled flow rate would give the best possible IMS sensitivity on today's 24-24-24 time basis, but less than 1 percent better than 8-56-8.
- Row Q shows that increasing the flow rate from two times current flow to three times current flow (Row R) is of very diminished value, and could save some energy.

5.3.1.4 Special Radiation Detection Modifications

Morris et al. 2017 investigated several options and their impact on power, air flow, spectral background, energy resolution (FWHM), geometric efficiency ($\varepsilon\delta\Omega$), and ultimately the MDC of the measurement. Some of the most powerful results come from increasing air flow or reducing the measurement background.

Table 5.4. Impacts on MDC for Several Variations in Design, Including Diverse Detector Types. Note that lower MDC is better.

Technology	Power	Air Flow	Background	Energy Resolution	Geometric Efficiency	MDC
Lower Resistance Filters	72%	100%				100%
Electrostatic Pretreatment Filter	73%	250%				62%
Electrostatic Precipitation (Low Power)	33%	100%				100%
Electrostatic Precipitation (High Flow)	100%	300%				58%
Particle Size Separation (Impactor)		100%				33% to 83%
Microcalorimeter	166%			9%	63%	38%
CZT	93%			335%	313%	104%
High Pressure Xenon	93%			779%	125%	250%
Sample Geometry (1 fold)					200%	71%
Sample Geometry (compression into puck)					500%	45%
Cosmic Veto			30%			45%
Compton Suppression			42%			65%
Gamma-Gamma Coincidence			40%			63%

This page intentionally left blank.

6.0 Conclusions

A few indisputable facts have been collected in the process of considering design options for a next-generation RASA:

- RASA could be optimized to deliver value in a wider range of scenarios while still delivering the classic IMS function.
- Greater sensitivity, earlier results, lower power, higher reliability, more location capability, and less reliance on expensive follow-up laboratories are all possible in a modular way.
- Developments in electrostatic precipitation could allow the RASA to collect a larger sample for less power.
- A range of possible operational schemes is possible with this new RASA.
- Converting the notional design developed here to a real design, optimized for various simultaneous needs, is still ahead of us.

There is still work to be done to determine if the individual ideas here interfere with or magnify the benefits of other improvements. Improved radiation detection simulations may improve our MDC theory section above, but actual measurements would be more satisfying than the formulaic approach of Section 5.4.1 or simulations, if possible. Further chemistry and gamma background investigations are needed to make sure the aluminum does not degrade RASA capabilities.

This page intentionally left blank.

7.0 References

Aalseth CE, RM Bonicaizi, MG Cantaloub, AR Day, LE Erikson, J Fast, JB Forrester, ES Fuller, BD Glasgow, LR Greenwood, EW Hoppe, TW Hossback, BJ Hyronimus, ME Keillor, EK Mace, JI McIntyre, JH Merriman, AW Myers, CT Overman, NR Overman, ME Panisko, A Seifert, GA Warren, and RC Runkle. 2012. "A shallow underground laboratory for low-background radiation measurements and materials development." *Review of Scientific Instruments*, 83(11):113503. doi:10.1063/1.4761923.

Aalseth C, E Andreotti, D Arnold, J-A Sanchez Cabeza, D Degering, A Giuliani, R Gonzales de Orduña, R. Gurriaran, M Hult, M Keillor, M Laubenstein, G le Petit, R Mircea Margineanu, M Matthews, H Miley, I Osvath, M Pellicciari, W Plastino, H Simgen, M Weber, and R Werzi. 2009. "Ultra-low background measurements of decayed aerosol filters." *Journal of Radioanalytical and Nuclear Chemistry*, 282(3):731-735. doi:10.1007/s10967-009-0307-0.

Biegalski SR, TW Bowyer, PW Eslinger, JI Friese, LR Greenwood, DA Haas, JC Hayes, I Hoffman, M Keillor, HS Miley, and M Morig. 2012. "Analysis of data from sensitive U.S. monitoring stations for the Fukushima Dai-ichi nuclear reactor accident." *Journal of Environmental Radioactivity*, 114:15-21. doi:10.1016/j.jenvrad.2011.11.007.

Brauer FP, JH Kaye, and JE Fager. 1975. "NaI(Tl)-Ge(Li) Coincidence Gamma-Ray Spectrometry for Radionuclide Analysis of Environmental Samples." *IEEE Transactions on Nuclear Science*, 22(1):661-670.

Burnett JL and AV Davies. 2014. "Cosmic veto gamma-spectrometry for Comprehensive Nuclear-Test-Ban Treaty samples." *Nuclear Instruments and Methods in Physics Research, Section A: Accelerators, Spectrometers, Detectors and Associated Equipment*, 747: 37-40.

Burnett JL, IM Cameron, and JL Slack. 2017. *Preliminary Report: US International Monitoring System Multi-Mission Data Study*. PNNL-27049, Pacific Northwest National Laboratory, Richland, Washington. (Limited distribution, unpublished)

Cochet R. 1961. "Lois Charge Des Fines Particules (Submicroniques) Etudes Theoriques—Controles Recents Spectre De Particules." *Coll. Int. la Physique des Forces Electrostatiques et Leurs Application, Centre National de la Recherche Scientifique, Paris*, 102:331–338.

Cooperman, G. 1981 "New Current-Voltage Relation for Duct Precipitators Valid for Low and High Current Densities." *IEEE Transactions on Industry Applications*, IA-17(2):236-9.

Cooperman P. 1960. "A Theory for Space-Charge-Limited Currents with Application to Electrical Precipitation." *Transactions of the American Institute of Electrical Engineers*, 79:47-50.

Currie LA. 1968. "Limits for Qualitative Detection and Quantitative Determination: Application to Radiochemistry." *Analytical Chemistry* 40(3):586-593. doi:10.1021/ac60259a007.

Eslinger PW and BT Schrom. 2016. "Multi-detection events, probability density functions, and reduced location area." *Journal of Radioanalytical and Nuclear Chemistry*, 307(3):1599-1605. doi:10.1007/s10967-015-4339-3.

Forrester JB, TW Bowyer, FF Carty, L Comes, PW Eslinger, LR Greenwood, DA Haas, JC Hayes, RR Kirkham, EA Lepel, KE Litke, HS Miley, SJ Morris, BT Schrom, P Van Davelaar, and VT Woods. 2011. *Lessons Learned In Aerosol Monitoring with the RASA.* PNNL-SA-82609, Pacific Northwest National Laboratory, Richland, Washington. https://www.ldeo.columbia.edu/res/pi/Monitoring/Doc/Srr_2011/PAPERS/04-11.PDF

Greenwood LR, MG Cantaloub, JL Burnett, AW Myers, CT Overman, JB Forrester, BG Glasgow, and HS Miley. 2017. "Low-background gamma-ray spectrometry for the international monitoring system." *Applied Radiation and Isotopes*, 126:240-242.

Hubbard JA, DK Wiemann, JS Wheeler, MA Omana, and JL Gerard. 2017. "Aerosol filtration testing for enhanced performance of radionuclide monitoring stations." *Journal of Radioanalytical and Nuclear Chemistry*, 314(2):1319-1336. doi:10.1007/s10967-017-5506-5.

Kalinowski MB and J Schulze. 2002. "Radionuclide monitoring for the Comprehensive Nuclear-Test Ban Treaty." *Journal of Nuclear Materials Management,* 30. 57-67. https://www.researchgate.net/profile/Martin_Kalinowski/publication/279907796_Radionuclide_monitoring_for_the_Comprehensive_Nuclear_Test_Ban_Treaty/links/562283ff08aed8dd194400c6.pdf

Le Petit, G, G Douysset, G Ducros, P Gross, P Achim, M Monfort, P Raymond, Y Pontillon, C Jutier, X Blanchard, T Taffary, and C Moulin. 2014. "Analysis of Radionuclide Releases from the Fukushima Dai-Ichi Nuclear Power Plant Accident Part I," *Pure and Applied Geophysics* 171(3-5):629-644. doi:10.1007/s00024-012-0581-6.

LeppÄnen A and H Toivonen. 1996. "Detection of man-made gamma-emitting radionuclides in the presence of radon progeny aerosols." In *Nucleation and Atmospheric Aerosols*, M Kulmala and PE Wagner (Eds.), Pergamon, Amsterdam, pp. 674-677.

Miley HS, CE Aalseth, TW Bowyer, JE Fast, JC Hayes, EW Hoppe, TW Hossback, ME Keillor, JD Kephart, JI McIntyre, and A Seifert. 2009. "Alternative treaty monitoring approaches using ultra-low background measurement technology." *Applied Radiation and Isotopes*, 67(5):746-749. doi:10.1016/j.apradiso.2009.01.069.

Miley HS. SM Bowyer, CW Hubbard, AD McKinnon, RW Perkins, RC Thompson, and RA Warner. 1998. "A description of the DOE Radionuclide Aerosol Sampler/Analyzer for the Comprehensive Test Ban Treaty." *Journal of Radioanalytical and Nuclear Chemistry*, 235(1-2):83-87. doi:10.1007/BF02385942.

Miley HS, SM Bowyer, CW Hubbard, AD McKinnon, RW Perkins, RC Thompson, and RA Warner. 1997. "Automated aerosol sampling and analysis for the Comprehensive Test Ban Treaty." In *1997 IEEE Nuclear Science Symposium Conference Record*, Vol 1:779-785. doi: 10.1109/NSSMIC.1997.672698.

Morris SJ, JL Burnett, and HS Miley. 2017. "Next-generation Radionuclide Aerosol Sampling and Measurement: Prospective Technologies." PNNL-SA-26377. Pacific Northwest National Laboratory, Richland, Washington. (Limited distribution, unpublished).

Parker, KR, ed. 1997. *Applied Electrostatic Precipitation*, Blackie Academic & Professional, London.

Perkins RW, DE Robertson, CW Thomas, and JA Young. 1990. "Comparison on nuclear accident and nuclear test debris." In *Proceedings of the International symposium on environmental contamination*

following a major nuclear accident, Vienna, Austria 16-20 Oct 1989. IAEA-SM--306/125, International Atomic Energy Agency, Vienna, Austria.

Reeves JH, RJ Arthur, and RL Brodzinski. 1992. "Sensitivity of LDEF Foil Analyses Using Ultra-low Background Germanium vs. Large NaI(Tl) Multidimensional Spectrometers." Presented at the Second LDEF Post-Retrieval Symposium June 1-5, 1992, San Diego, California. https://digital.library.unt.edu/ark:/67531/metadc710470/

Singlevich W. 1948. *Radioactive contamination in the environs of the Hanford Works for the period April - May - June, 1948*. HW-11333, General Electric Company, Hanford Works, Washington. doi:10.2172/6371269.

Thompson RC, HS Miley, and RJ Arthur. 2002. *Filter Media Recommendation Review*. PNNL-13754. Pacific Northwest National Laboratory, Richland, Washington. doi: 10.2172/890735.

Wogman NA, RW Perkins, and JH Kaye. 1969. "An all sodium iodide anticoincidence shielded multidimensional gamma-ray spectrometer for low-activity samples." *Nuclear Instruments and Methods*, 74(2): 197-212. doi:10.1016/0029-554X(69)90337-1.

This page intentionally left blank.

Appendix A

Mylar Chemistry Experiments

This page intentionally left blank.

Appendix A

Mylar Chemistry Experiments

A sample of Mylar material was received to test the current ability of the PNNL radiochemistry program-approved processes and chemists to analyze the material. Traditionally, samples are separated prior to analysis, which requires samples to be dissolved and homogenized into a solution. Two methods validated to achieve solutions are dry ashing and wet ashing (chemical dissolution without aid of dry ashing). These methods will be tested for their ability to achieve a solution suitable for processing, but no chemical separations will be performed.

The sample received consisted of 10 layers of flat Mylar, heat-sealed on opposite ends. Theoretically the Mylar is coated on one side with aluminum, although it was not clear which side was coated, as they appeared to be the same. No information was given as to the layer thickness of the aluminum, which made estimating sample size difficult for solubility; note that a Material Safety Data Sheet would likely be useful for making this estimation. Sections were cut from the heat-sealed end for testing and weights were taken to compare sub-samples on a per gram basis. The sample size was approximately 2.5 inches x 10.5 inches, heat-sealed on one end to hold the 10 layers together. Six sub-samples were cut from this original sample, two for dry ashing tests in a muffle furnace and four for chemical treatments and heat testing. The details of each sub-sample are shown in Table A.1, however only one of the samples for dry ashing was tested.

Table A.1. Sample Variables and Treatments

Sample Name	Mass (g)	Parameter	Time and Temperature in Degrees Celsius
Al-my-1	2.98663	Muffle	1 h @ 200, 2 h @ 500, 2 h @ 1000
Hydrochloric Acid	2.98845	Conc. Rgt. Grade	1 h @ room temp, 1 h @ 150
Water	3.17585	NANOPURE	1 h @ room temp, 1 h @ 150
Nitric Acid	3.13949	Conc. Rgt. Grade	1 h @ room temp, 1 h @ 150
Fuming Nitric Acid	3.33851	Concentrated	1 h @ room temp, 1 h @ 150

Conc. = Concentrated, Rgt. = Reagent

Immediately upon the addition of the solutions to the Mylar, the fuming nitric acid (roughly 90 percent HNO_3) was reacting with the surface and the shiny appearance started to look like a ball of crumpled aluminum foil as seen in Figure A.1D. The concentrated nitric acid (roughly 70 percent HNO_3) was reacting slightly (Figure A.1C) and the concentrated hydrochloric acid was showing small cracks on the surface of the Mylar (Figure A.1A). The water had no reaction initially (Figure A.1B).

After the first hour at room temperature, the metallic finish on the Mylar had effectively reacted with the hydrochloric acid and the plastic backing could be seen with bubbles in Figure A.2A. The concentrated nitric acid was starting to react and the solution was turning yellow while the surface of the Mylar was crinkled and etched (Figure A.2C). In fuming nitric acid, the Mylar was starting to lose its structural integrity (Figure A.2D).

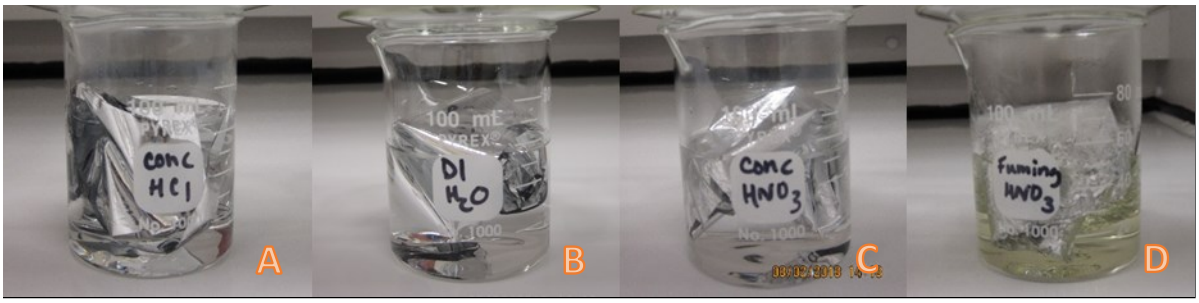

Figure A.1. Initial Samples at Room Temperature with Reagents Added. Beaker A contains hydrochloric acid (HCl), beaker B contains water (H_2O), beaker C contains concentrated nitric acid (HNO_3), and beaker D contains fuming nitric acid.

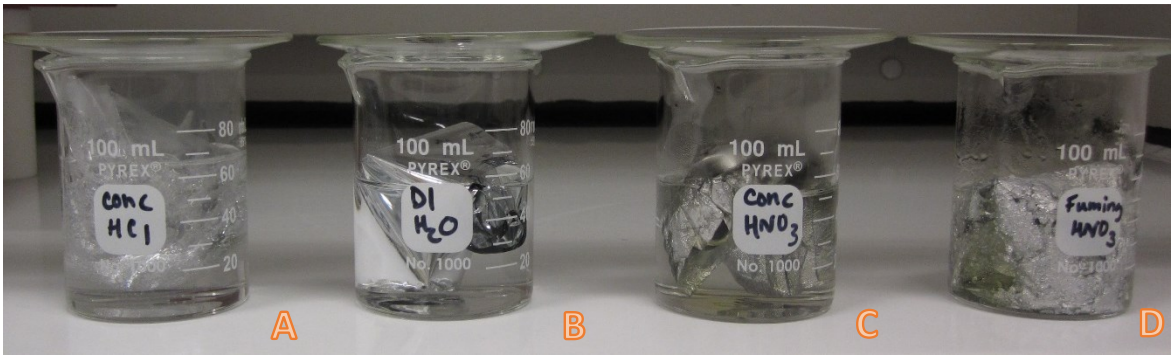

Figure A.2. Mylar Samples in Reagents after 1 Hour at Room Temperature

In Figure A.3, the Mylar samples were heated at 150^{0}C. The concentrated nitric acid reacted with the surface of the Mylar and turned black as wisps of (presumably) the aluminum went into solution almost immediately. The fuming nitric acid turned the Mylar into a sparkly soupy mess. It was not clear if the Mylar was in solution or if the aluminum coating had flaked off and was swirling around the solid material. The hydrochloric acid sample showed little to no changes visible, as the metallic finish on the Mylar had dissolved at room temperature previously.

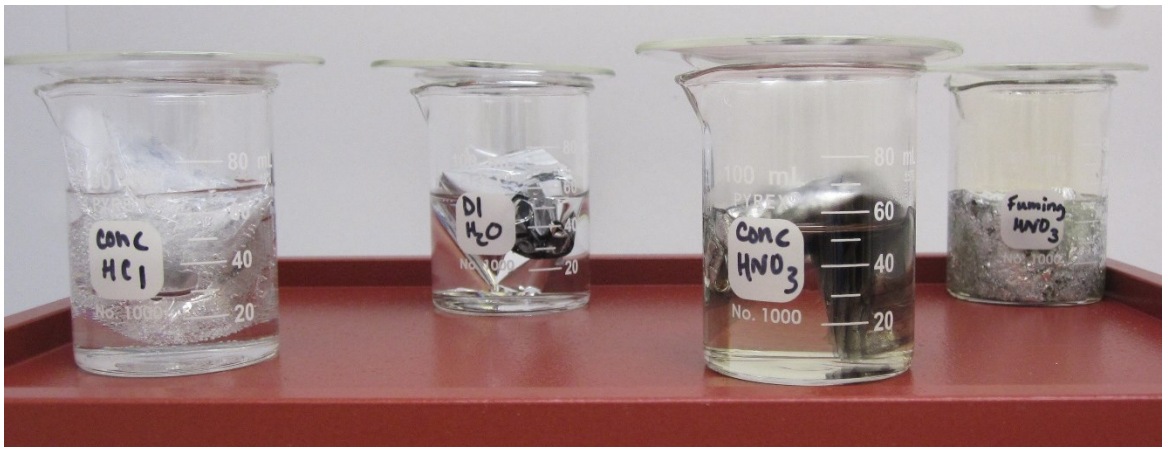

Figure A.3. Mylar Samples in Reagents after Heating at 150^{0}C for 5 minutes

After heating for about 20 minutes, the metallic finish on the Mylar in concentrated nitric acid was gone and in fuming nitric acid, the Mylar appear to be totally dissolved at first glance. Upon further inspection, the organic remnants of the Mylar could be seen floating around as a suspension in the solution. It also appeared that the metallic finish in the water sample was disappearing. At this point pH measurements of the solution in the water sample were taken, and indicated an approximate pH of 3. This could be caused by the acid fumes of the HCl or HNO_3 depositing in the water sample, so it was relocated to the front of the hotplate to limit this interaction. Figure A.4 shows the comparison of the hot samples.

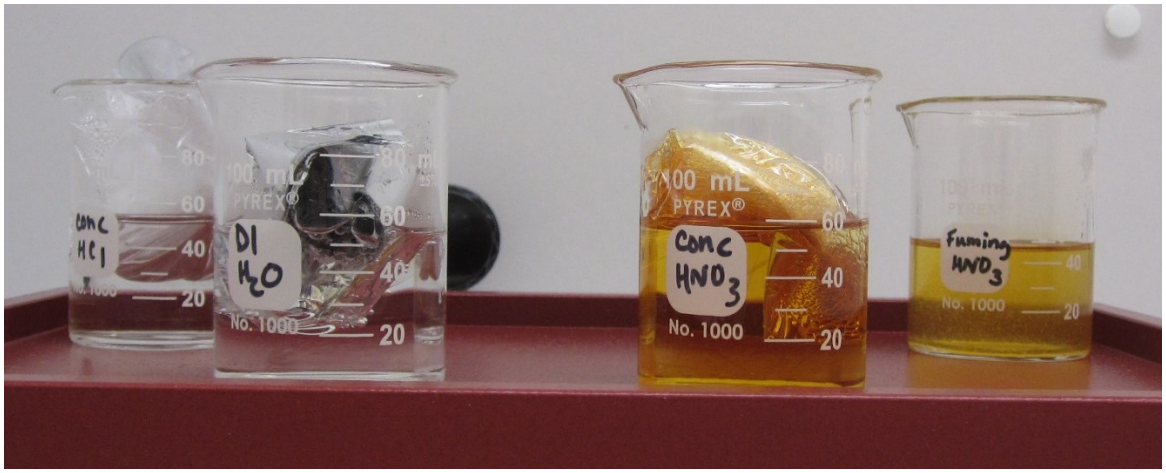

Figure A.4. Mylar Samples in Reagents after Heating at 150^0C for 20 minutes

As the reagents were evaporated, the water sample lost all of the metallic sheen on the Mylar. The concentrated nitric acid continued to degrade the Mylar while heating, but did not evaporate as fast as the other samples, likely due to vapors being trapped in the film that did not dissolve and formed a layer on the top of the solution. Swirling the sample helped agitate the sample and release some of the NO_x vapors, but the sample did not reduce in volume any further. In Figure A.5, the hydrochloric acid and water samples are clearly reacting differently than the nitric acid samples.

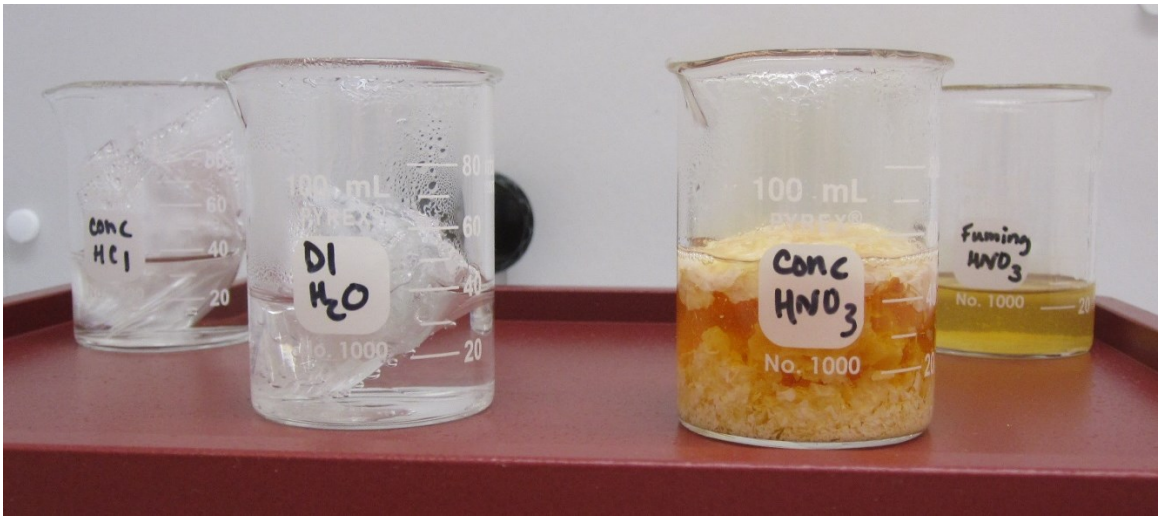

Figure A.5. Evaporating Reagents with Mylar Samples

After heating the samples for more than two hours, the water had evaporated completely while the concentrated HCl only reduced in volume. The concentrated nitric acid had some evaporative loss, but was significantly impaired and did not substantially reduce in volume. The fuming nitric acid sample had more solids crashing out of solution than expected as it approached dryness. The residue could not be digested completely with additional fuming nitric acid, but could potentially be soluble with a perchloric acid treatment. It is unclear what the constituents of the remaining material were and therefore perchloric acid will not be used at this time to ensure safe chemical digestions. Standard chemical dissolution methods employ nitric, hydrochloric, and perchloric acid but the perchloric acid is only used once the organic material is mostly gone. In this case, it was not clear if the residue was from organic decomposition products from the Mylar or from something in the coating. Figure A.6 shows the solution of Mylar after being digested for two hours with heat.

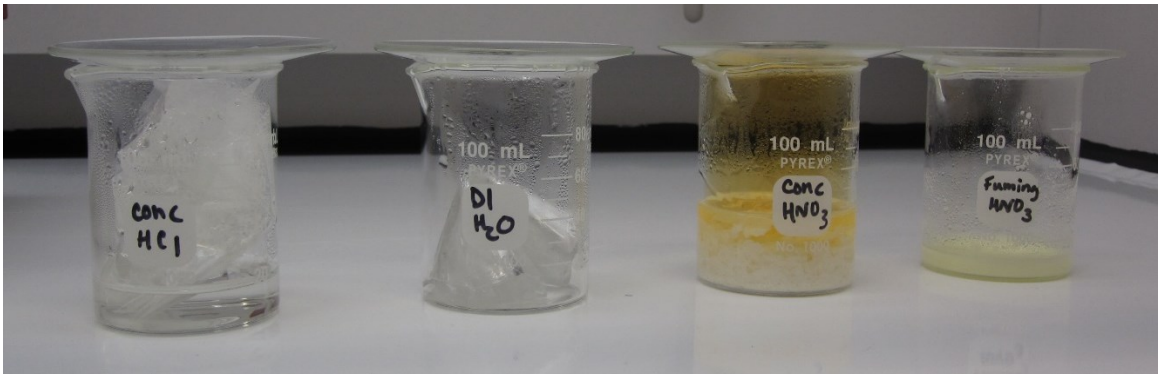

Figure A.6. Mylar Samples in Reagents after Evaporating for 2 Hours

The Al-my-1 sample was heated in a muffle furnace for one hour at 100^0C, then ramped to 200^0C and heated for another hour. A programming error occurred on the furnace and it did not complete the desired range of temperatures. Upon returning to the lab, the furnace was at room temperature and the sample was charred but not ashed. The furnace was then ramped to 500^0C and left for two hours at that temperature before ramping to 1000^0C and holding for another two hours. At the completion of the program, the sample was white, but had not ashed as expected. Upon adding fuming nitric acid to the ash, the residue floated and did not dissolve. This was suspected to be due to the aluminum film being insoluble in nitric acid. The sample was then transposed to a hydrochloric acid system; however, the sample ash still did not dissolve. Figure A.7 shows the residue of the ashed Mylar sample Al-my-1 after transposition to hydrochloric acid and evaporation; note the chunky residue left behind.

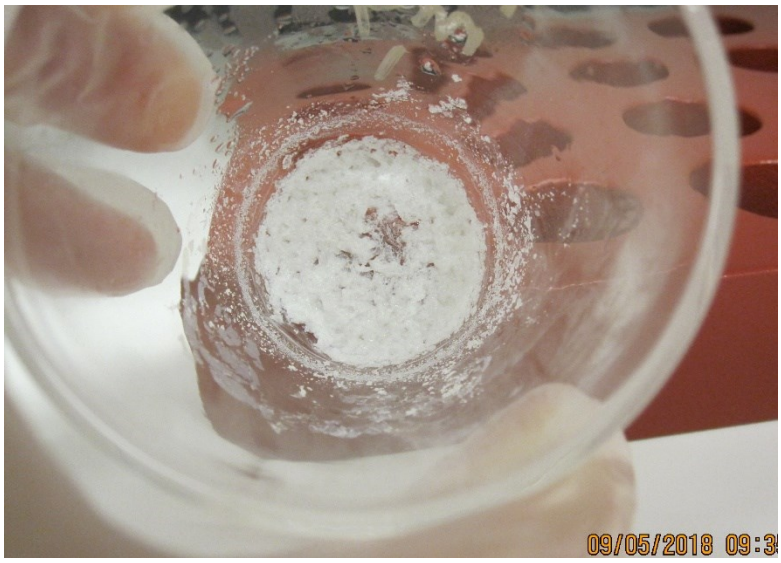

Figure A.7. Ashed Mylar Sub-sample Al-my-1 in Hydrochloric Acid Residue

Pacific Northwest
NATIONAL LABORATORY

www.pnnl.gov

902 Battelle Boulevard
P.O. Box 999
Richland, WA 99352
1-888-375-PNNL (7665)

U.S. DEPARTMENT OF
ENERGY